

Article

# Method for Estimating Optimal Position of S-Band Relay Station through Path Loss Analysis in an Outdoor Environment

Doyoung Jang <sup>1</sup>, Sungsik Wang <sup>1</sup>, Chun Won Kim <sup>2</sup>, Yong Bae Park <sup>3</sup> and Hosung Choo <sup>1,\*</sup>

<sup>1</sup> School of Electronic and Electrical Engineering, Hongik University, Seoul 04066, Korea; dyjang1224@mail.hongik.ac.kr (D.J.); kingwss@mail.hongik.ac.kr (S.W.)

<sup>2</sup> Naro Space Center, Korea Aerospace Research Institute, Goheung, Jeollanam-do 59569, Korea; chunwon@kari.re.kr

<sup>3</sup> Department of Electrical and Computer Engineering, Ajou University, Suwon, Gyeonggi-do 16499, Korea; yong@ajou.ac.kr

\* Correspondence: hschoo@hongik.ac.kr

Received: 16 July 2020; Accepted: 29 August 2020; Published: 2 September 2020



**Featured Application:** This article is related to estimation method to optimize position of a relay station in the S-band.

**Abstract:** This article investigates a novel estimation method to optimize the position of a relay station of the S-band telemetry system in outdoor environments. To determine an optimal relay station position, complex terrain surface and buildings near the Naro Space Center are included in the EM (Electromagnetic) simulation. The optimal relay station position is then determined using the estimation method by comparing the path losses from the rocket to the main station and some candidate positions of the relay station. To better understand the path loss, the ray analysis is also conducted, and the result demonstrates that once the rocket altitude to be covered by the relay station is determined, it is possible to find the optimum position of the relay station.

**Keywords:** electromagnetic wave propagation; wireless communications; ray tracing method; relay station

## 1. Introduction

Along with the recent widespread expansion of aerospace applications, the demand for a variety of wireless communication technologies is gradually increasing in rocket launch events [1–3]. The wireless communication systems are generally used for collecting the information about the rocket status [4–6]. If the communication link between the rocket and the main station is disconnected, the rocket's position can be missed. Then, the rocket should self-destruct for safety issue with a termination command. Thus, maintaining a stable communication link is critical for successful rocket launch events. However, due to the reflection and diffraction from complex terrain and buildings, the radio propagation characteristics may be significantly degraded in outdoor environments [7–11]. Moreover, the environment where the communication is taking place changes rapidly depending on the altitude of the launched rocket. Previously, electric field distributions by wireless communication systems were analyzed in outdoor wave propagation studies [12,13], and a path loss model for the urban area was proposed [14–16]. Channel characteristics analysis for moving targets including line of sight (LoS) and non-line of sight (NLoS) situations was also executed [17–19]. However, research on the propagation characteristics from the launched rocket to the base station or the relay station according to the altitude of the rocket has not been fully carried out yet.

In this paper, we propose a novel estimation method to optimize a relay station position of the S-band telemetry system in outdoor environments. The estimation method using the EM simulation needs four steps: first, the model for the nearby environment such as the terrain and building is included in the EM simulation. Second, the path loss between the rocket and the receiver according to rocket's altitude is calculated using the EM simulation. Third, the optimal position of the relay station is determined by examining the path loss from the rocket to the relay station and the main station. Finally, the optimum position of the relay station is validated by observing the effect of the radiation pattern and phase variation. To determine an optimal relay station position, a ray tracing-based EM simulation software (Wireless InSite) is utilized [20], complex terrain surfaces and buildings near the Naro Space Center are included in the simulation. The transmitting and receiving antenna patterns are also considered in the simulation. Their radiation patterns are assumed to be a dipole pattern and an ideal isotropic pattern, respectively. The optimal relay station position is then determined using the estimation method by comparing the path losses from the rocket to the main station and some candidate positions of the relay station. The relay station in this work is not portable and should be installed at a fixed position on a building. The rocket's communication link is significantly influenced by the surrounding terrain and buildings, especially when the rocket is at low altitudes. Since the shorter distance between the transmitting and receiving antennas has a lower path loss, the relay station near the rocket is more advantageous for maintaining a better communication link. However, when the rocket is at high altitude, the gain in the LoS direction decreases due to the weak pattern of the antenna in the rocket's tail direction. Thus, it is very important to select the advantageous position of the relay station for a better overall communication link. The results demonstrate that the relay stations near the rocket are more advantageous when the rocket's altitude is low due to less path loss. On the other hand, due to the shaded region by the radiation pattern of the transmitting antenna, the relay station farther away would be better for the rocket at a higher altitude. It means that once the rocket altitude to be covered by the relay station is determined, it is possible to find the optimum position of the relay station. The presented method for determining the optimal position of the relay station can be practically applied in aerospace applications. To better understand the resulting path losses, we observed several ray paths from the rocket to the relay stations. We found that slow envelope variations and fast fluctuations in the received power are due to the transmitting antenna pattern and the phase difference between the direct and indirect reflected rays, respectively. Based on this path loss analysis, according to the rocket's altitude, it is possible to determine the optimal relay position considering the outdoor environment near the rocket launch site.

## 2. Path Loss Simulation for Optimal Relay Position

Figure 1 presents the configuration of the S-band telemetry system for rocket launching, where the main station and the relay station are used simultaneously to receive status information from the rocket. Immediately after launching the rocket, detailed status information of the rocket is broadcasted, and the main station should consistently receive the information to monitor the rocket status without interruption. However, since the rocket, when at lower altitudes, is significantly influenced by the terrain and nearby buildings, the communication link between the rocket at lower altitude and the main station can be seriously affected. In order to maintain a stable communication link, it is necessary to place an additional relay station at a location where the path loss is lower than at the main station.

The altitude of the rocket is denoted by  $h$ , and the distance from the rocket to the relay station and the main station is indicated by  $d_R$  and  $d_M$ , respectively. As  $h$  increases, the radio wave shading region is widened due to the weak radiation pattern of the transmitting antenna in the tail direction of the rocket. On the other hand, as  $d_R$  decreases, the path loss between the rocket and relay station becomes lower. The receiver closer to the rocket can have less path loss, but it may quickly enter the radio shaded area as the rocket altitude rises. Thus, the optimal additional receiver position should be determined considering the radio wave shaded area and distance between the rocket and the relay

station. Considering these issues, we investigated the optimal location of the relay station at the Naro Space Center in Korea.

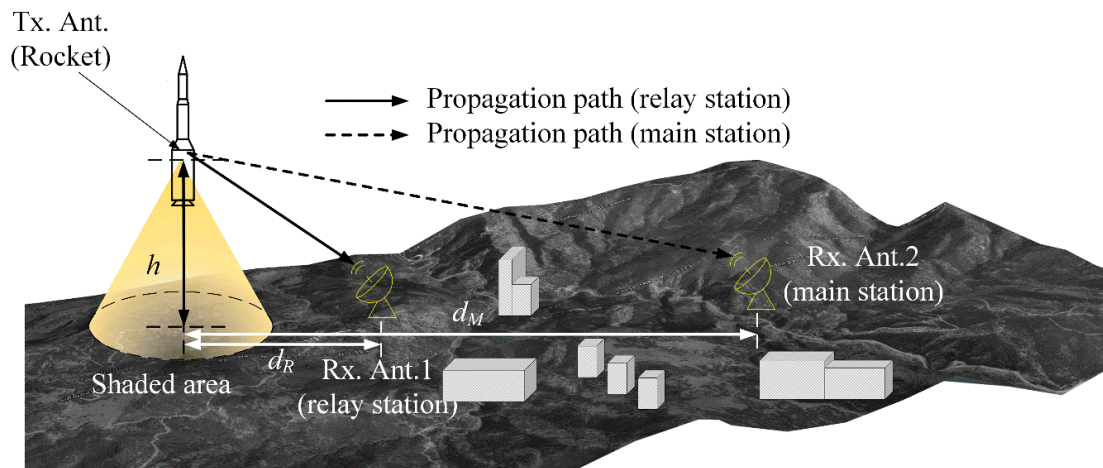


**Figure 1.** Configuration of the S-band telemetry system with main and relay stations.

Figure 2 shows detailed location information for the Naro Space Center on the eastern side of Oenaro-island. The analysis area is limited to a  $1.2 \times 2.4$  km range, including the Naro Space Center. Since this area is surrounded by various outdoor features such as the sea, terrain, and buildings, they are included as accurately as possible in our simulation, as shown in Figure 3.

Figure 3 shows the model for the EM analysis, which approximates the analysis area with triangular meshes, including the main station and the relay station. The four candidate locations of the relay stations that are determined considering the ease of placement are denoted by  $p_1$ ,  $p_2$ ,  $p_3$ , and  $p_4$ , and the main station is denoted by  $p_5$ . In this rocket launch scenario, the position of the main station is given previously. However, in this work, the position of the relay station can be changed. The relay station just plays the role that supports the main station when it is difficult for the main station to receive signals. The relay station can maintain a communication link with the rocket when a received power of more than  $-100$  dBm is obtained by the receiving antenna. Thus, it is very important to select the advantageous position of the relay station for a better overall communication link. Of the candidate locations, the position  $p_1$  is closest to the rocket and the position  $p_4$  is closest to the main station. The detailed coordinate parameters for the candidate positions and the main station are listed in Table 1. To calculate the path losses from the rocket to the candidate relay station, a ray tracing-based EM simulation software (Wireless InSite [20]) is utilized along with the model shown in Figure 3. The transmitting and receiving antenna patterns are also included in the simulation. The transmitting antenna is assumed to be a half-wavelength dipole antenna with vertical polarization, and it is also assumed that there is no pattern distortion caused by the rocket. Therefore, maximum gain is 2.15 dBi, and radiation pattern is omni-directional pattern in the azimuth direction with a half-power beam width of  $90^\circ$  in the elevation direction. Simultaneously, we use the receiving antenna with an ideal isotropic pattern, which helps to observe the effect by the surrounding environment without the influence of the antenna pattern itself.

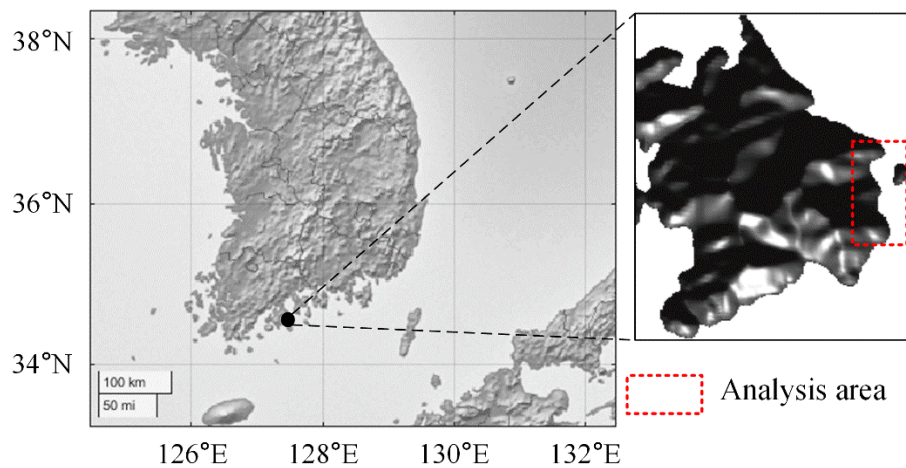


Figure 2. Location of the Naro Space Center and the analysis area.

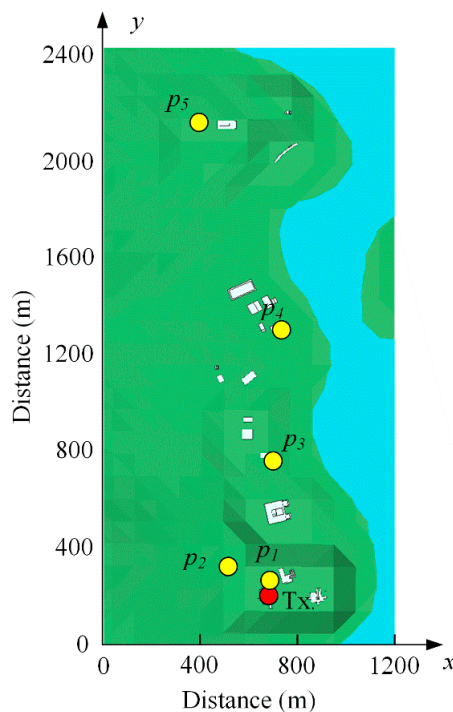


Figure 3. Simulation model for analysis area.

Table 1. Coordinates of the main station and candidate positions of the relay stations.

Symbols	Coordinates	Distance (Tx. to Rx.)
$p_1$	$(x,y) = (689 \text{ m}, 237 \text{ m})$	50 m
$p_2$	$(x,y) = (521 \text{ m}, 292 \text{ m})$	198 m
$p_3$	$(x,y) = (671 \text{ m}, 767 \text{ m})$	581 m
$p_4$	$(x,y) = (707 \text{ m}, 1290 \text{ m})$	1104 m
$p_5$ (main station)	$(x,y) = (711 \text{ m}, 2097 \text{ m})$	1952 m

Figure 4 illustrates the path loss distributions in the analysis area at rocket altitudes of 0 m and 1000 m. To obtain the simulated result, up to 25 rays are calculated between the transmitting antenna and the receiving antenna. In addition, we arranged receivers at 10 m intervals in the analysis area, and the altitude is limited to less than 1000 m, because the communication link is more significantly influenced by the surrounding terrain surface and buildings, especially when the rocket is at a low altitude. When the rocket’s altitude is 0 m, the path loss at  $p_1$  is the lowest among all the candidate

positions, as shown in Figure 4a. As can be seen, some areas around the basin and buildings have a higher path loss due to the lack of LoS between the rocket and observation points. On the other hand, at a rocket altitude of 1000 m, those areas can have a better LoS, resulting in lower path loss, as shown in Figure 4b.

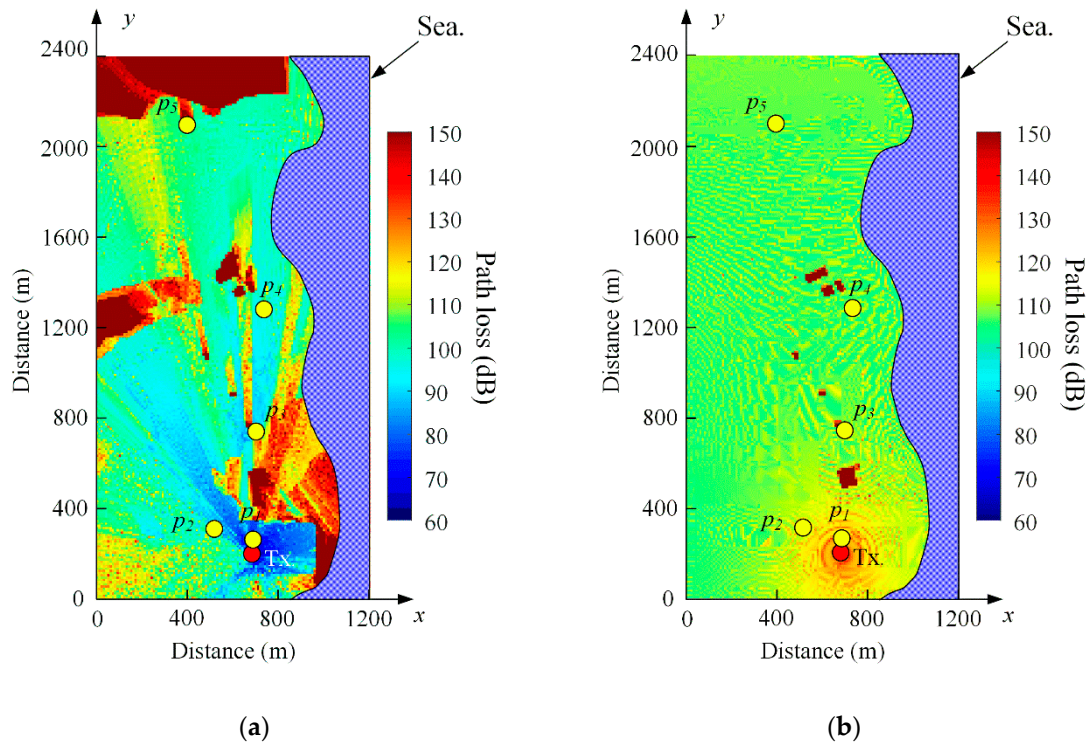


Figure 4. Path loss distributions according to rocket altitude: (a) at 0 m; (b) at 1000 m.

Figure 5 presents the path loss at the main station and the candidate positions along the altitude of the rocket. To obtain this result, we simulated the path loss between the rocket and the relay station by varying the rocket’s altitude from 0 m to 1000 m with an increment of 1 m. The black line shows the path loss of the main station, and other color lines indicate the path loss of the candidate positions  $p_1$ ,  $p_2$ ,  $p_3$ , and  $p_4$ , respectively. The path loss at the four candidate positions have different rate increase of along the rocket altitude, and thus the path losses of four candidate positions intersect with the path loss of the main station at different rocket height. The altitude of the rocket where the path loss intersects between the candidate site and the main station is very important. Below the crossing altitude the reception is dominantly handled by the relay station, above which the main station is responsible for reception. Therefore, once the rocket altitude that the relay station will receive is determined, the optimal position of the relay station can also be decided. However, since there are fast fluctuations in the path loss, it is difficult to obtain the rate of increase and the interaction altitude. Therefore, the running average was applied to the path loss result to facilitate the acquisition of the rate of increase and intersection altitude.

Figure 6 represents the running averaged path losses at the main station and the candidate positions along the rocket altitude using the running average as shown in the following equation [21]:

$$x_i(K) = \frac{1}{K} \sum_{k=t_0+1}^{t_0+K} x_i(k) \tag{1}$$

where  $x_i$  is original data, and  $K$  is the window size in which the sample values are averaged. In this work,  $K$  is selected as 100. As shown in Figure 6, the running averaged data  $x_i(K)$  becomes smoother, and the crossing altitude is also more clearly observed. For the candidate position  $p_1$ , since  $p_1$  is the

closest point to the rocket, the lowest path loss is observed at  $p_1$  as indicated with a blue line when  $h$  is near an altitude of 0 m. However, the path loss increases rapidly with the rocket altitude, and the crossing altitude is relatively low at 217 m. Thus, it is more advantageous to receive the rocket status from the relay station than the main station when the rocket altitude is under  $h = 217$  m. On the other hand, in case of the position  $p_4$ , which is the farthest point from the rocket, the pass loss increases slowly according to  $h$ . Thus, the relay station at  $p_4$  is more suitable for reception than the main station when the rocket altitude is under 1000 m.  $p_2$  and  $p_3$  are placed between  $p_1$  and  $p_4$  so that the intersection altitudes at these positions are 432 m and 619 m, respectively. The relay stations at  $p_2$  and  $p_3$  have are advantageous than the main station when rocket altitudes are less than 432 m and 619 m, respectively. Therefore, once the rocket altitude to be covered by the relay station is determined, it is possible to find the optimum position of the relay station. In our rocket launching event, the rocket altitude covered by the relay station is assumed to be 430 m. Thus,  $p_2$  is found to be the optimum position of the relay station.

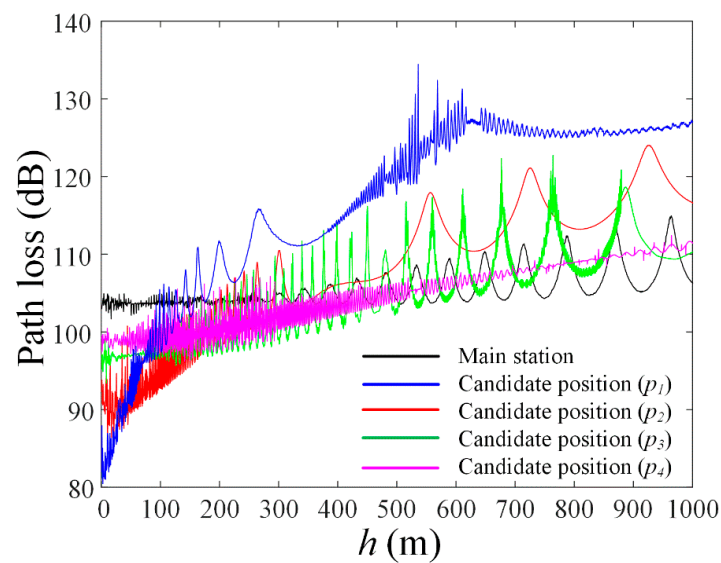


Figure 5. Path loss according to rocket's altitude.

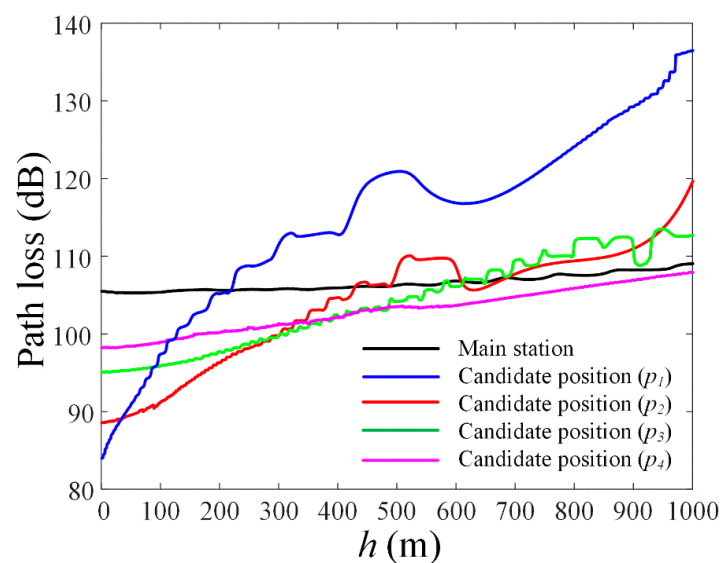


Figure 6. Running averaged path loss according to rocket's altitude.

### 3. Verification Using Ray Analysis

To validate the result in Figure 5, we compare the received power at the optimum position  $p_2$  along the rocket altitude with the gain of the transmitting antenna. Figure 7 illustrates the relation between the elevation angle and the rocket's altitude in the LoS direction at  $p_2$ . The blue line expresses the radiation pattern of the transmitting antenna, and the elevation angle at the LoS direction is denoted by  $\theta_e$ , which is related to the rocket's altitude of  $h$ . For example, as  $\theta_e$  increases according to the rocket altitude  $h$ , the gain along the LoS direction decreases due to the weak pattern of the antenna in the rocket's tail direction.

Figure 8 presents the elevation angle and the gain according to the rocket's altitude. The solid line presents  $\theta_e$  along  $h$ , and the dashed line indicates the LoS direction's gain along  $h$ . As can be seen in Figure 8,  $\theta_e$  increases from  $-3.6$  to  $78.7^\circ$  when the rocket's altitude  $h$  increases from 0 to 1000 m. At the same time, the gain in the LoS direction decreases from 2.15 to  $-12.0$  dBi. Thus, the  $\theta_e$  is proportional to the rocket's altitude, and the gain decreases with the rocket's altitude. The result demonstrates that gain in the LoS direction is related to radiation pattern of the transmitting antenna and rocket's altitude, because the relation of the  $\theta_e$  and the gain in the LoS direction is determined by transmitting antenna pattern. Therefore, it can be expected that the increments in path loss are mainly influenced by the radiation pattern of the transmitting antenna, as the rocket's altitude increases.

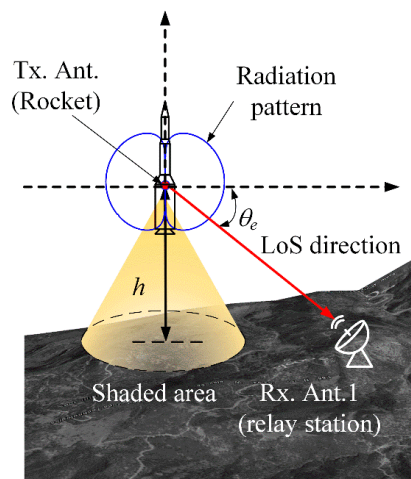


Figure 7. Relation between the elevation angle and the rocket's altitude in the LoS direction.

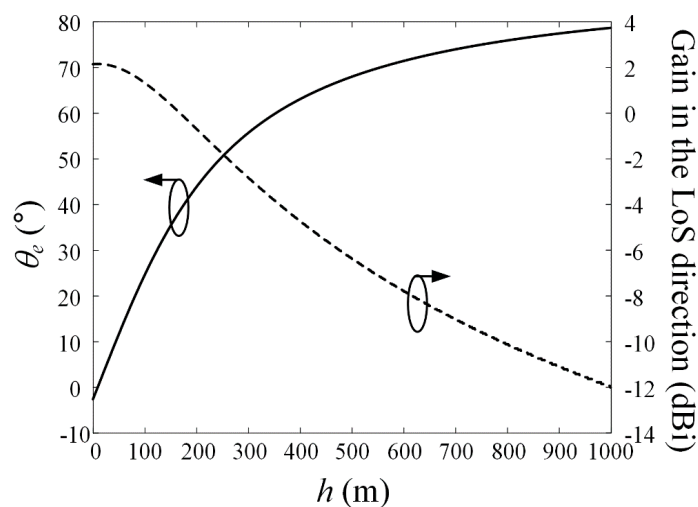


Figure 8. Elevation angle and the gain according to the rocket's altitude.

The Figure 9 shows the received power and the gain in the LoS direction at  $p_2$ . The solid line shows the received power when the input power to the transmitting antenna in the rocket is 0 dBm. The received power is  $-86$  dBm at the altitude of 200 m where the path loss is 86 dB. Thus, the received power in Figure 9 is related to the path loss in Figure 5. The dashed line is the antenna gain of the transmitting antenna in the rocket along the LoS direction according to the altitude. Therefore, we found that the envelope of the received power curve is very similar to the gain curve in the LoS direction according to the altitude  $h$ . The envelope of the received power gradually decreases due to the weak radiation pattern of the transmitting antenna in the tail direction of the rocket when the rocket's altitude increases.

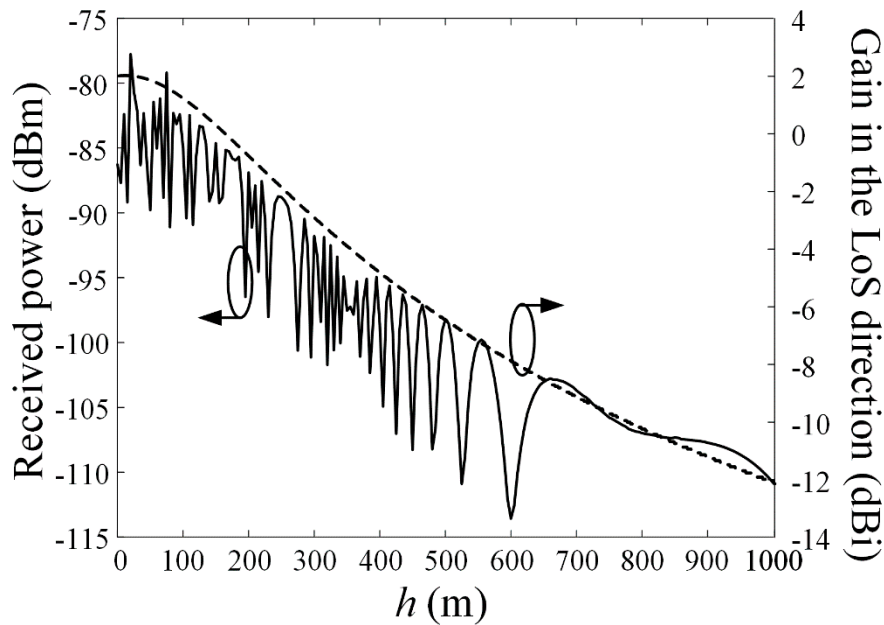


Figure 9. Received power and the gain in the LoS direction at  $p_2$ .

Figure 10 describes the received power intensity and phase differences between direct and reflected rays, which can be written as Equations (2) and (3), respectively [22]:

$$E_d^k = |E_1^k| e^{-j\beta\phi_d} \tag{2}$$

where  $E_d$  is the electric field of a direct ray, which is generally dominant, and the superscript  $k$  is the index of the observed point.  $E_m$  represents the total multiple reflected rays, which can be expressed as below:

$$\begin{aligned} E_m^k &= |E_2^k| \left\{ \prod_{n=1}^{N_2} (|\Gamma_{(2,n)}| e^{-j\phi_{(2,n)}}) \right\} e^{-j\beta\phi_2} \\ &+ |E_3^k| \left\{ \prod_{n=1}^{N_3} (|\Gamma_{(3,n)}| e^{-j\phi_{(3,n)}}) \right\} e^{-j\beta\phi_3} \\ &+ |E_4^k| \left\{ \prod_{n=1}^{N_4} (|\Gamma_{(4,n)}| e^{-j\phi_{(4,n)}}) \right\} e^{-j\beta\phi_4} \\ &= |E_m^k| e^{-j\beta\phi_m} \end{aligned} \tag{3}$$

where  $N_p$  represents the number of  $p$ th rays so that  $|\Gamma_{(p,n)}|$  and  $\phi_{(p,n)}$  are the amplitude and phase of  $n$ th reflection coefficients for the  $p$ th ray.

$$\angle\Phi^k(\phi) = \phi_d - \phi_m \tag{4}$$

where  $\Phi_k$  is the phase difference between the phase  $\phi_d$  of the direct ray and the phase  $\phi_m$  of the summation of the multiple reflected rays. The higher phase difference results in the lower the received power. Therefore, from the results, it can be understood that the slow envelope variation of the received

power arises from the antenna radiation pattern in the LoS direction, and the fast fluctuation of the received power comes from the phase difference between the direct and reflected rays.

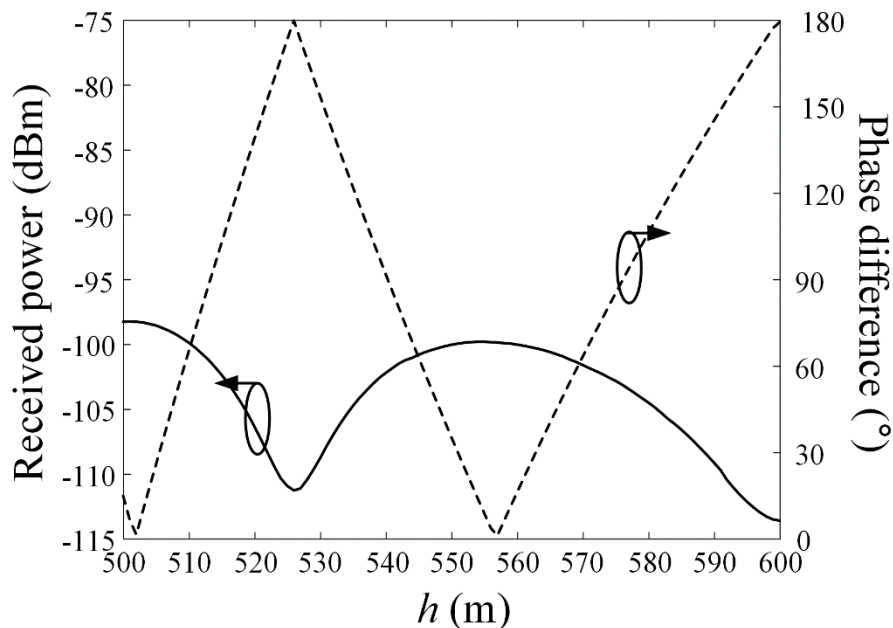


Figure 10. Received power and the phases difference between the direct and reflected rays.

#### 4. Drawbacks

Unfortunately, we have limited information for the telemetry system used in this work due to the security concerns. Since we did not show specific information of all systems used, our paper may seem somewhat superficial. The restrictions of our paper are as follows: first, detailed information for transmitter and receiver is not included. Second, the size and geometry of the main structures are not shown. Finally, accurate frequency information is not released. Nevertheless, we have tried our best to explain detailed information about the system as possible in our paper.

#### 5. Conclusions

We have investigated a novel estimation method to optimize the position of a relay station of the S-band telemetry system in outdoor environments. The optimal relay station position was then determined using the estimation method by comparing the path losses from the rocket to the main station and some candidate positions of the relay station. The path loss at the four candidate positions had different rates of increase along the rocket altitude, and thus, it intersected with the path of the main station at different rocket height. Therefore, once the rocket altitude that the relay station would receive was determined, the optimal position of the relay station could also be decided. To verify the result, the received power at the optimum position along the rocket altitude was examined by comparing it with the gain of the transmitting antenna. From the results, it could be understood that the slow envelope variation of the received power arises from the antenna radiation pattern in the LoS direction, and the fast fluctuation of the received power came from the phase difference between the direct and reflected rays. The proposed method can also be applied to the cell planning applications in mobile communications because mobile communications require many repeaters at high heights.

**Author Contributions:** Conceptualization, D.J., S.W., C.W.K., and H.C.; methodology, D.J. and S.W.; software, D.J.; validation, D.J., S.W., C.W.K., Y.B.P., and H.C.; formal analysis, D.J. and S.W.; investigation, D.J. and S.W.; writing—original draft preparation, D.J. and S.W.; writing—review and editing, D.J., Y.B.P., and H.C.; visualization, D.J.; supervision, H.C.; project administration, H.C.; funding acquisition, H.C. All authors have read and agreed to the published version of the manuscript.

**Funding:** This research received no external funding.

**Conflicts of Interest:** The authors declare no conflict of interest.

## References

1. Rice, M.; Hogstrom, C.; Afran, M.S.; Saquib, M. On sparse channel estimation in aeronautical telemetry. *IEEE Trans. Aerosp. Electr. Syst.* **2019**, *55*, 2612–2618. [[CrossRef](#)]
2. Shi, X.; Shen, Y.; Wang, Y.; Bai, L. Differential-clustering compression algorithm for real-time aerospace telemetry data. *IEEE Access* **2018**, *6*, 57425–57433. [[CrossRef](#)]
3. Afran, M.S.; Saquib, M.; Rice, M. On the effects of channel sparsity on joint estimators in aeronautical telemetry. *IEEE Trans. Aerosp. Electr. Syst.* **2020**, *56*, 2507–2514. [[CrossRef](#)]
4. Lancelle, D.-M.; Božić, O.; Köke, H. Flight test results of the investigation of acceleration effects on a gun-launched rocket engine. *IEEE Trans. Plasm. Sci.* **2013**, *41*, 1364–1369. [[CrossRef](#)]
5. Fowler, T.C.R.S. A six-channel high-frequency telemetry system. *IRE Trans. Space Eleletr. Telem.* **1960**, *6*, 69–81. [[CrossRef](#)]
6. Dent, A.E.; Rae, W.M.; White, J.H. Some telemetry systems for space research. *J. Br. Inst. Radio Eng.* **1961**, *22*, 465–476. [[CrossRef](#)]
7. Blaunstein, N.; Yarkoni, N.; Katz, D. Spatial and temporal distribution of the VHF/UHF radio waves in built-up land communication links. *IEEE Trans. Antenn. Propag.* **2006**, *54*, 2345–2356. [[CrossRef](#)]
8. O'Brien, W.M.; Kenny, E.M.; Cullen, P.J. An efficient implementation of a three-dimensional microcell propagation tool for indoor and outdoor urban environments. *IEEE Trans. Vehic. Technol.* **2000**, *49*, 622–630. [[CrossRef](#)]
9. Fernandes, L.C.; Soares, A.J.M. Simplified characterization of the urban propagation environment for path loss calculation. *IEEE Antennas Wirel. Propag. Lett.* **2010**, *9*, 24–27. [[CrossRef](#)]
10. You, J.W.; Cui, T.J. Efficient approach to accurately analyze wireless propagation and fading in time domain. *IEEE Antennas Wirel. Propag. Lett.* **2016**, *15*, 1767–1770. [[CrossRef](#)]
11. Nam, J.-H.; Rim, J.-W.; Lee, H.; Koh, I.-S.; Song, J.-H. Modeling of monopulse radar signals reflected from ground clutter in a time domain considering Doppler effects. *J. Electromagn. Eng. Sci.* **2020**, *20*, 190–198. [[CrossRef](#)]
12. Lee, Y.S.; LEE, H.-S.; Choi, H.-D. A study on the convenient EMF compliance assessment for base station installations at a millimeter wave frequency. *J. Electromagn. Eng. Sci.* **2018**, *18*, 242–247. [[CrossRef](#)]
13. Xu, P.; Lam, K.W.; Tsang, L.; Lai, K.L. Statistical Distributions of Fields in Urban Environment Based on Monte Carlo Simulations of Maxwell Equations. *IEEE Antennas Wirel. Propag. Lett.* **2004**, *3*, 34–37.
14. Andrusenko, J.; Miller, R.L.; Abrahamson, J.A.; Emanuelli, N.M.M.; Pattay, R.S.; Shuford, R.M. VHF general urban path loss model for short range ground-to-ground communications. *IEEE Trans. Antennas Propag.* **2008**, *56*, 3302–3309. [[CrossRef](#)]
15. Zhang, X.; Andrews, J.G. Downlink cellular network analysis with multi-slope path loss models. *IEEE Trans. Commun.* **2015**, *63*, 1881–1894. [[CrossRef](#)]
16. Kim, K.W.; Oh, S.-J. Geometric Optics-Based Propagation Prediction Model in Urban Street Canyon Environments. *IEEE Antennas Wirel. Propag. Lett.* **2015**, *15*, 1128–1131. [[CrossRef](#)]
17. Wu, Z.-H.; Lou, Y.; Yung, M.E.K.-N. Channel measurement, simulation, and analysis for high-speed railway communications in 5G millimeter-wave band. *IEEE Trans. Intell. Transp. Syst.* **2018**, *19*, 3144–3158.
18. Wei, W.; Shi, J.; Jiang, M.; Che, H.; Chen, L. Dynamic Simulation and Performance Optimization of Wireless Communication in Urban Rail Transportation. In Proceedings of the 2013 IEEE International Conference on Intelligent Rail Transportation, Beijing, China, 11–13 December 2013.
19. Yu, J.; Chen, W.; Li, F.; Li, C.; Yang, K.; Liu, Y.; Chang, F. Channel Measurement and Modeling of the Small-Scale Fading Characteristics for Urban Inland River Environment. *IEEE Trans. Wire Commun.* **2020**, *19*, 3376–3389. [[CrossRef](#)]

20. Remcom: Wireless InSite. 2019. Available online: <http://www.remcom.com/wireless-insite> (accessed on 31 December 2019).
21. Zhu, S.; Soh, Y.C.; Xie, L. Distributed parameter estimation with quantized communication via running average. *IEEE Trans. Sign. Proc.* **2015**, *63*, 4634–4646. [[CrossRef](#)]
22. Jang, D.; Youn, S.; Park, J.-E.; Choo, J.; Choo, H. Electromagnetic field propagation and indoor exclusion zone analysis in a nuclear power plant. *IEEE Trans. Electromagn. Compat.* **2020**, *99*, 1–8. [[CrossRef](#)]



© 2020 by the authors. Licensee MDPI, Basel, Switzerland. This article is an open access article distributed under the terms and conditions of the Creative Commons Attribution (CC BY) license (<http://creativecommons.org/licenses/by/4.0/>).